Corepressor SMRT promotes oxidative phosphorylation in adipose tissue and protects against diet-induced obesity and insulin resistance

Sungsoon Fang[a], Jae Myoung Suh[a], Annette R. Atkins[a], Suk-Hyun Hong[a], Mathias Leblanc[a], Russell R. Nofsinger[a], Ruth T. Yu[a], Michael Downes[a], and Ronald M. Evans[a,b,1]

[a]Gene Expression Laboratory, Salk Institute for Biological Studies, La Jolla, CA; and [b]Howard Hughes Medical Institute, Salk Institute for Biological Studies, La Jolla, CA 92037

Contributed by Ronald M. Evans, December 1, 2010 (sent for review November 15, 2010)

The ligand-dependent competing actions of nuclear receptor (NR)-associated transcriptional corepressor and coactivator complexes allow for the precise regulation of NR-dependent gene expression in response to both temporal and environmental cues. Here we report the mouse model termed silencing mediator of retinoid and thyroid hormone receptors (SMRT)^{mRID1} in which targeted disruption of the first receptor interaction domain (RID) of the nuclear corepressor SMRT disrupts interactions with a subset of NRs and leads to diet-induced superobesity associated with a depressed respiratory exchange ratio, decreased ambulatory activity, and insulin resistance. Although apparently normal when chow fed, SMRT^{mRID1} mice develop multiple metabolic dysfunctions when challenged by a high-fat diet, manifested by marked lipid accumulation in white and brown adipose tissue and the liver. The increased weight gain of SMRT^{mRID1} mice on a high-fat diet occurs predominantly in fat with adipocyte hypertrophy evident in both visceral and s.c. depots. Importantly, increased inflammatory gene expression was detected only in the visceral depots. SMRT^{mRID1} mice are both insulin-insensitive and refractory to the glucose-lowering effects of TZD and AICAR. Increased serum cholesterol and triglyceride levels were observed, accompanied by increased leptin and decreased adiponectin levels. Aberrant storage of lipids in the liver occurred as triglycerides and cholesterol significantly compromised hepatic function. Lipid accumulation in brown adipose tissue was associated with reduced thermogenic capacity and mitochondrial biogenesis. Collectively, these studies highlight the essential role of NR corepressors in maintaining metabolic homeostasis and describe an essential role for SMRT in regulating the progression, severity, and therapeutic outcome of metabolic diseases.

metabolic syndrome | chronic inflammation | transcriptional repression

Metabolic syndrome, a Western diet-induced proinflammatory disease affecting up to 25% of Americans, is characterized by impaired glucose tolerance, central obesity, dyslipidemia, insulin resistance, and type 2 diabetes. Secondary complications associated with metabolic syndrome include atherosclerosis, stroke, fatty liver disease, blindness, and others (1, 2). Several members of the nuclear receptor (NR) family of transcription factors have been implicated in the progression of metabolic syndrome, including the peroxisome proliferator-activated receptors (PPARs), retinoic acid receptors (RARs), and thyroid hormone receptors (TRs) (3). NRs direct transcriptional activation or repression of target genes through ligand-dependent association of coactivator or corepressor complexes, respectively, that covalently modify histone sites within chromatin (4, 5). NR-mediated transcriptional activation has well-established roles in development, xenobiotic and inflammatory responses, and metabolic homeostasis. In contrast, the role of NR-mediated transcriptional repression in whole-body physiology and homeostasis is less well understood (6, 7). The use of genetic loss-of-function knock-in models that target NR corepressor associations allows for the direct interrogation of the global role of NR repression in both development and metabolic homeostasis. Two prototypical NR corepressors, silencing mediator of retinoid and thyroid hormone receptors (SMRT) and nuclear receptor corepressor (NCoR), interact with NRs through corepressor/nuclear receptor (CoRNR) box motifs in their receptor interaction domains (RIDs) (8–10). Knock-in mutations of critical residues in the two RIDs of SMRT selectively disrupted NR–SMRT interactions. Mice bearing these mutations (SMRT^{mRID}) had widespread metabolic defects including reduced respiration, altered insulin sensitivity, and increased adiposity (11). In another study, a liver-specific deletion of two of NCoR's RIDs revealed a critical role for NCoR-mediated repression in both TR and liver X receptor (LXR) gene regulation (12). However, the dysregulation seen in each of these mouse models developed on a chow diet unlike classic metabolic disease that depends on environmental stressors such as a high-fat diet.

Chronic inflammation has been established as a common feature of the metabolic syndrome, in which the combinatorial effects of cytokine/chemokine induction are associated with metabolic dysregulation (13). In metabolic syndrome, lipids can serve dually as ligands that initiate both the innate immune response (e.g., TLR4) and metabolic regulation (e.g., PPARs and LXRs). TLR4 activation is required for the development of vascular inflammation and insulin resistance in diet-induced obesity models (14). Regular exercise offers protection against chronic inflammation through the release of myokines (including IL-6, which induces fat oxidation) and anti-inflammatory cytokines (such as IL-1ra and IL-10) and inhibits the production of the proinflammatory cytokine TNFα (15). In contrast, a sedentary "couch potato" lifestyle is a feature of diet-induced obesity and insulin resistance, increasing the risk of chronic inflammation.

Here we report a mouse model in which disruption of a specific subset of SMRT–NR interactions results in phenotypes that mirror many of the risk factors associated with the development of the metabolic syndrome. These mice appear normal on a regular diet, but, when challenged by a high-fat diet, they become superobese and insulin-resistant. Our results indicate that SMRT-mediated NR repression may act as a protective mechanism in the body's defense against the environmental stressor of a high-fat diet. This study describes a model for metabolic disease and an essential role of the NR corepressor SMRT in regulating the progression, severity, and therapeutic outcome of the disease.

Author contributions: S.F., M.D., and R.M.E. designed research; S.F., J.M.S., S.-H.H., and R.R.N. performed research; S.F., J.M.S., A.R.A., M.L., R.T.Y., M.D., and R.M.E. analyzed data; and S.F., A.R.A., R.T.Y., M.D., and R.M.E. wrote the paper.

The authors declare no conflict of interest.

Freely available online through the PNAS open access option.

[1]To whom correspondence should be addressed. E-mail: evans@salk.edu.

This article contains supporting information online at www.pnas.org/lookup/suppl/doi:10.1073/pnas.1017707108/-/DCSupplemental.

Results

High-Fat Diet Induces Superobesity in SMRT^{mRID1} Knock-In Mice. Two-hybrid analysis confirmed that mutation of the RID1 domain clearly disrupts interaction with a select subset of nuclear receptors, including RAR and TR (Fig. S1). To study the in vivo role of SMRT-RID1–dependent nuclear receptor repression, we generated knock-in mice (SMRT^{mRID1}) harboring alanine mutations in the SMRT-RID1 domain via site-specific mutagenesis (Fig. 1*A*). We obtained germline transmission of the SMRT-RID1 knock-in allele, and heterozygous crosses yielded all three genotypes in a Mendelian ratio. During embryonic development and at birth, the homozygous SMRT^{mRID1} mice on a C57Bl6/J background were viable and identical to wild-type (WT) and heterozygote littermates in size and weight. Micro CT scan revealed that there was no difference in bone between WT and SMRT^{mRID1} (Fig. S2). The expression levels of endogenous SMRT did not change in many tissues from SMRT^{mRID1} mice compared with WT. We measured the growth rate of SMRT^{mRID1} mice and observed that they attained body weights similar to WT for 11 mo after birth on normal chow (NC). However, when placed on a high-fat diet (HFD), SMRT^{mRID1} mice nearly doubled the weight gain (15 vs. 29 gm) of their WT littermates, resulting in a superobese phenotype (Fig. 1 *B* and *C*). Echo MRI body composition analysis showed that nearly all of the additional weight gain in SMRT^{mRID1} mice was in adipose and not lean mass (Fig. 1*D*). With the notable exception of epididymal fat pads, all white and brown fat depots from SMRT^{mRID1} mice were significantly increased in mass relative to WT (Fig. 1*E*).

HFD Induces Adiposity-Associated Inflammation in SMRT^{mRID1} Mice. An increase of white adipose tissue mass can occur by hyperplastic or hypertrophic growth. Histological analysis demonstrated that the cross-sectional area of adipocytes from visceral fat pads, both epididymal and mesenteric, in SMRT^{mRID1} mice were increased relative to WT, whereas cells from the s.c. inguinal fat pad in SMRT^{mRID1} mice were relatively smaller (Fig. 1 *F* and *G*; Fig. S3). Because obesity is often accompanied by tissue inflammation, we examined the expression levels of inflammatory cytokines in white adipose tissue (WAT) depots. Consistent with our histology data, a large number of inflammatory cytokines in visceral mesenteric fat were found to be significantly increased in HFD-fed SMRT^{mRID1} mice. In contrast, decreased expression was observed in the inguinal fat pads from these mice. Accordingly, macrophage marker F4/80 expression was significantly increased only in visceral fat pads, suggesting that macrophage infiltration plays a key role in the induction of an inflammatory response in visceral fat (Fig. S4). These findings suggest that SMRT may attenuate the inflammatory response of visceral WAT to a HFD (Fig. 1*H*).

HFD-Induced Hepatic Steatosis in SMRT^{mRID1} Mice. Obesity in humans as well as in animal models is often associated with hepatic steatosis or fatty liver disease. Consistent with this phenotype, large lipid vesicles were observed in the hepatocytes of HFD-fed SMRT^{mRID1} mice (Fig. 2*A*), which exhibited a doubling in liver weight compared with HFD WT mice (Fig. 2*B*). In accord with hematoxylin and eosin staining, hepatic lipid analysis showed a dramatic increase in triglyceride (TG) and cholesterol levels in the HFD-SMRT^{mRID1} liver compared with the HFD-WT liver (Fig. 2*C*). Furthermore, HFD-SMRT^{mRID1} mice showed increased serum alanine aminotransferase (ALT) levels, a sign of HFD-induced liver damage (Fig. 2*D*). Consistent with the above phenotype, expression analysis revealed changes in liver-relevant NRs [increased PPARγ, LXRα, decreased small heterodimer partner (SHP)] and their target genes, including a marked induction of

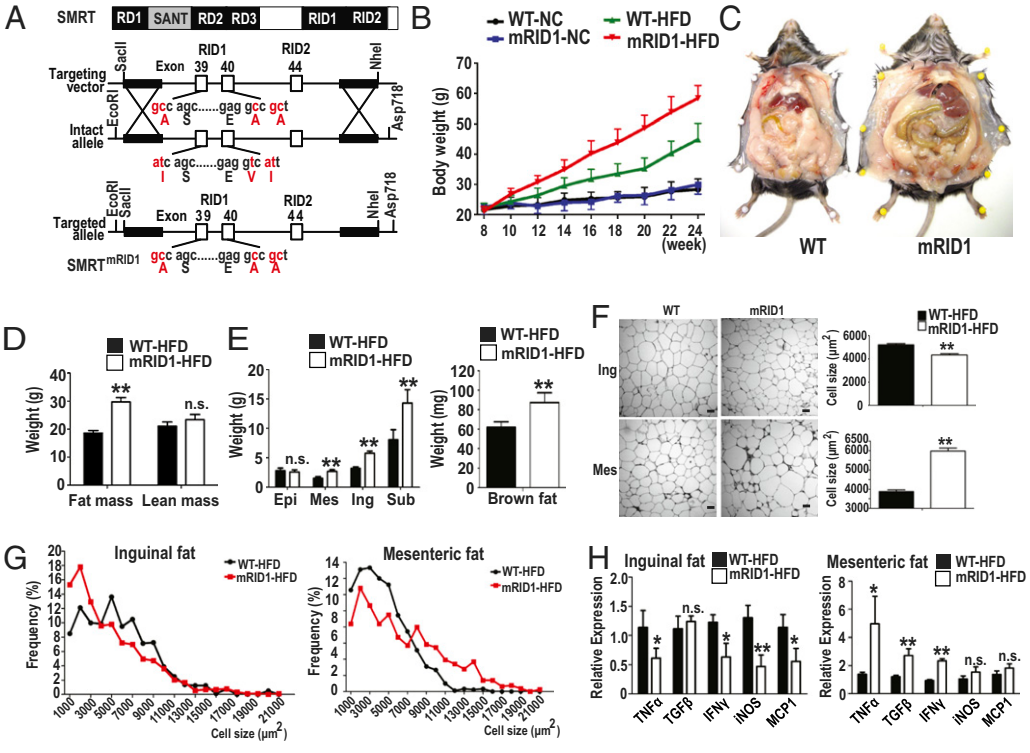

Fig. 1. HFD-induced severe obesity in SMRT^{mRID1} mice. (*A*) Generation of SMRT^{mRID1} mutant knock-in mice. (*B*) Bodyweight curves in WT and SMRT^{mRID1} on normal chow or HFD. (*C*) WAT accumulation in 14-wk HFD-treated WT and SMRT^{mRID1} mice. (*D*) Body weight composition of WT and SMRT^{mRID1} mice. (*E*) Wet weight of epididymal (Epi), mesenteric (Mes), inguinal (Ing), subcutaneous (Sub), and brown fat (BAT) depots in WT and SMRT RID1 mice. (*F* and *G*) Hematoxylin and eosin staining of histological sections and adipocyte cross-sectional area from WAT depots in WT and SMRT^{mRID1} mice. (Scale bar, 50 μm.) (*H*) Expression of inflammatory cytokines in WAT from WT and SMRT^{mRID1} mice. All error bars are SD. *$P < 0.05$; **$P < 0.01$; n.s., not significant unless otherwise indicated.

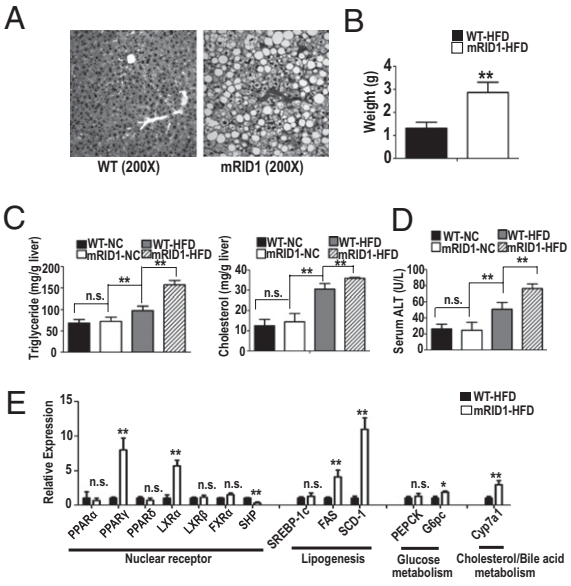

Fig. 2. HFD-induced liver steatosis in SMRT^{mRID1} mice. (*A*) Hematoxylin and eosin staining of histological sections from liver in HFD-challenged WT and SMRT^{mRID1} mice. (*B*) Liver weight was increased in SMRT^{mRID1} mice. (*C*) The levels of hepatic triglyceride and cholesterol in WT and SMRT^{mRID1} mice (n = 5). (*D*) The level of serum ALT in WT and SMRT^{mRID1} mice (n = 5). (*E*) Hepatic gene expression of nuclear receptors, lipogenesis, glucose, and cholesterol/bile acid metabolism in WT and SMRT^{mRID1} mice. All error bars are SD. *P < 0.05; **P < 0.01; n.s., not significant.

a variety of LXR-regulated lipogenic genes and the induction of CYP7a1 upon reduction in SHP levels in the HFD-SMRT^{mRID1} liver (Fig. 2*E*), indicating that SMRT repression helps to protect against diet-induced liver damage.

Impaired Glucose Homeostasis in SMRT^{mRID1} Mice. Obesity is associated with elevated serum lipids and predisposes rodents and humans to impaired glucose homeostasis. We find that dysfunction of the RID1 domain results in the exacerbation of both conditions upon challenge with a HFD. SMRT^{mRID1} mice display a 100% elevation of cholesterol (Fig. 3*A*), a 55% increase in serum triglycerides (Fig. 3*B*), a 12-fold induction in fasting insulin levels (Fig. 3*C*), and a 4-fold rise in leptin (Fig. 3*D*). In each case, the HFD-WT levels were also increased but to a significantly lower extent. In contrast to the above changes, we found that adiponectin levels were reduced in HFD-fed SMRT^{mRID1} mice (Fig. 3*E*) whereas free fatty acid (FFA) levels did not change (Fig. 3*F*). These data suggest that elevated endogenous insulin levels might be compensating for peripheral insulin resistance in HFD-fed SMRT^{mRID1} mice. We therefore performed glucose tolerance tests (GTTs) and insulin tolerance tests (ITTs) to determine whether glucose homeostasis was impaired in HFD-fed SMRT^{mRID1} mice. Intraperitoneal challenge of mice with 2 g/kg glucose demonstrated glucose intolerance and insulin resistance in HFD-fed SMRT^{mRID1} mice (Fig. 3 *G* and *H*). Interestingly, NC-fed SMRT^{mRID1} mice exhibited no difference in glucose homeostasis compared with NC-fed WT mice (Fig. S5). Antidiabetic drugs have been shown to improve glucose tolerance in rodents and humans. To determine whether antidiabetic drugs improve glucose homeostasis in SMRT^{mRID1} mice, we tested whether an i.p. injection of the PPARγ agonist rosiglitazone (5 mg/kg) or the AMPK agonist AICAR (250 mg/kg) could lower blood glucose. WT mice showed a rapid and sustained reduction in blood glucose level in response to rosiglitazone (Fig. 3*I*) and AICAR (Fig. 3*J*). Unexpectedly, the SMRT^{mRID1} mice were largely refractory to both insulin sensitizers (Fig. 3 *I* and *J*), indicating that the SMRT-RID1 domain is needed to defend against diet-induced insulin resistance and to confer responsiveness to insulin-sensitizing drugs.

SMRT Controls Energy Expenditure. As both PPARγ and AMPK activity are known regulators of energy expenditure and thermogenesis, we next investigated the thermogenic capacity and energy balance of SMRT^{mRID1} mice. Large lipid vesicles were observed in the brown adipose tissue (BAT) of SMRT^{mRID1} HFD-fed mice that were absent in HFD-fed WT (Fig. 4*A*). As

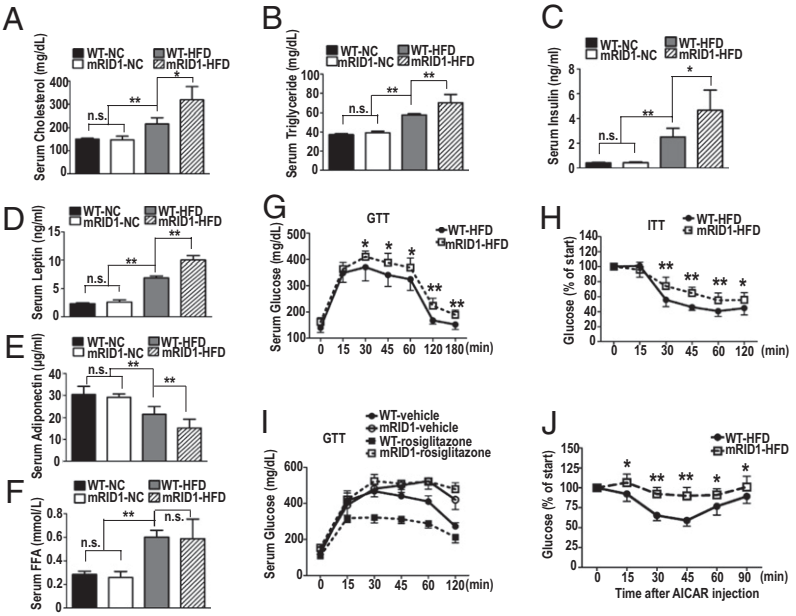

Fig. 3. HFD-induced perturbed metabolic phenotypes in SMRT^{mRID1} mice. (*A–F*) Fasting serum cholesterol, triglyceride, insulin, leptin, adiponectin, and free fatty acid in WT or SMRT^{mRID1} mice (n = 5). (*G*) Glucose tolerance test revealed increased fasting blood glucose and intolerance in SMRT^{mRID1} mice compared with WT (n = 8). (*H*) Insulin sensitivity test revealed reduced glucose clearance in SMRT^{mRID1} mice. (*I* and *J*) Blood glucose levels at indicated times in WT (n = 8) or SMRT^{mRID1} mice (n = 7) following i.p. injection of rosiglitazone (5 mg/kg) or AICAR (250 mg/kg). All error bars are SD. *P < 0.05; **P < 0.01; n.s., not significant.

BAT is a major tissue protecting against cold exposure, we examined whether lipid accumulation in BAT reduced thermogenesis in HFD-fed SMRT^{mRID1} mice. A small, although not statistically significant, reduction in resting body temperature was noted for the mutant mice (WT: 37.1 ± 0.25 °C; SMRT^{mRID1}: 36.3 ± 0.25 °C); however, the SMRT^{mRID1} mice exhibited significantly lower core body temperatures at all time points following acute cold exposure (Fig. 4*B*). Gene expression analysis confirmed that expression of PPARδ, ERRγ, and their coactivator PGC-1α, as well as a large number of their target genes involved in thermogenesis, mitochondrial biogenesis, and FA oxidation, was markedly reduced (Fig. 4*C*), suggesting that mitochondrial function in BAT is impaired in HFD-fed SMRT^{mRID1} mice. Although hyperphagia is a well-described phenotype in numerous rodent models of obesity, HFD-fed SMRT^{mRID1} mice actually consumed less food than HFD-fed WT mice (Fig. S6), indicating that obesity in SMRT^{mRID1} animals is likely due to reduced energy expenditure.

HFD Shifts Energy Metabolism from OXPHOS to Glycolysis in SMRT^{mRID1}. The observation that energy expenditure in brown fat is impaired in HFD-fed SMRT^{mRID1} mice led us to examine whether they have global metabolic defects. Although no obvious defects were observed in mice maintained on normal chow, HFD-fed SMRT^{mRID1} mice were found to produce far less CO_2 and consume less O_2 than WT mice (Fig. 5*A*), suggesting that oxidative phosphorylation is impaired by the disruption of the SMRT-RID1 domain. Furthermore, ambulatory counts for the mutant mice were dramatically reduced during the dark phase, when mice are normally active. Indeed, diet-induced sedentary behavior is so dramatic that SMRT^{mRID1} HFD-fed mice show even lower activity in the dark phase than in the light phase. This increased sedentary behavior of HFD-fed SMRT^{mRID1} mice suggested that they would have reduced energy expenditure in their skeletal muscle (Fig. 5*B*). Respiratory quotient (RQ) was lower in HFD-fed SMRT^{mRID1} mice during both light and dark phases (Fig. 5*C*), suggesting a preference for fatty acids as the metabolic substrate of choice or a relative resistance to carbohydrate metabolism. However, expression analysis of FA oxidation genes in skeletal muscle showed a robust suppression in HFD-fed SMRT^{mRID1} mice (Fig. 5*F*). Furthermore, CO_2 production and O_2 consumption were dramatically reduced in SMRT^{mRID1} mice (Fig. 5*A*), indicating that these mice have defects in both carbohydrate metabolism and FA oxidation for fuel utilization and are less energetic. Given the correlation of body weight with metabolic defects, it is possible that the reduced metabolic rates and activity of SMRT^{mRID1} mice may be a consequence of their increased obesity compared with WT mice. However, a comparison of body-weight–matched mice revealed significant reductions in the volume of CO_2 produced (VCO_2), the volume of O_2 consumed (VO_2), RQ, and ambulatory counts in SMRT^{mRID1} mice compared with WT (Fig. S7). This finding suggests that the reduced metabolic rates and activity of the SMRT^{mRID1} mice can be attributed to the disruption of RID1.

Next, we compared cellular bioenergetics by measuring oxidative consumption rates (OCR) and extracellular acidification rates (ECAR) (Seahorse Bioscience XF analyzer) that reflect OXPHOS and glycolytic metabolism, respectively, in stromal vascular fractions (SVF) from the epididymal fat of WT and SMRT^{mRID1} mice. These assays show that cellular energy metabolism was shifted from OXPHOS to glycolysis in HFD-fed SMRT^{mRID1} mice, suggesting that the SMRT-RID1 domain is critical for regulating oxidative metabolism (Fig. 5*D*). Consistent with this, serum lactate levels were significantly increased in HFD-fed SMRT^{mRID1} mice, suggesting that the whole-body energy metabolism is shifted from OXPHOS to glycolysis in HFD-fed SMRT^{mRID1} mice (Fig. 5*E*).

SMRT Regulates PGC-1α Expression. To further clarify the defects in oxidative metabolism and the shift to a more glycolytic energy metabolism, we examined gene expression levels of critical proteins in skeletal muscle. These studies revealed that the expression of uncoupling protein and FA oxidation genes were significantly reduced, whereas that of the key rate limiting the glycolytic gene PFK was significantly increased in HFD-fed SMRT^{mRID1} mice (Fig. 5*F*), without commensurate changes in the levels of relevant NRs. However, the expression of PGC-1α was markedly reduced, whereas PGC-1β was unchanged (Fig. 5*G*). This is consistent with the critical regulatory role of this NR coactivator in mitochondrial function (16, 17). It was recently reported that DNA methyltransferase 3b (DNMT3b) is a modulator that regulates the expression of PGC-1α (18). Interestingly, the expression of DNMT3b was significantly increased in HFD-fed SMRT^{mRID1} mice, suggesting that elevated DNMT3b would repress the expression of PGC-1α and thus result in reduced mitochondrial function (Fig. 5*G*).

Discussion

In its role as a NR corepressor, SMRT has been reported to function as a critical metabolic modulator regulating glucose metabolism, adipogenesis, and inflammation. Previously, we demonstrated that comprehensive ablation of SMRT–NR interactions (by mutation of both RID 1 and 2) severely disrupted metabolic homeostasis. Notably, the reduced respiration, altered insulin sensitivity, and increased adiposity phenotype of these double knock-in (DKI) mice were evident in chow-fed animals, that is, in the absence of an environmental stressor (11). Dysregulation of multiple receptor pathways, including those of TR and PPARγ, were identified as contributing to the phenotype of the DKI mice. In contrast, the single knock-in SMRT^{mRID1} mice, in which only selected SMRT–NR interactions were disrupted, did not exhibit any overt metabolic or inflammatory phenotype on a normal diet. However, when challenged with a high-fat diet, SMRT^{mRID1} mice displayed decreased ambulatory activity and developed superobesity and insulin resistance reminiscent of metabolic syndrome disease, but distinct from the DKI mice. The reduced energy expenditure of SMRT^{mRID1} mice was associated with decreased PGC1α expression in BAT and muscle, reduced uncoupling protein gene expression, and a switch to a more glycolytic state, indicative of reduced mitochondrial function. Furthermore, these mice had markedly increased inflammatory gene expression in the metabolically relevant visceral fat, suggesting that SMRT-mediated transcriptional repression of select NR

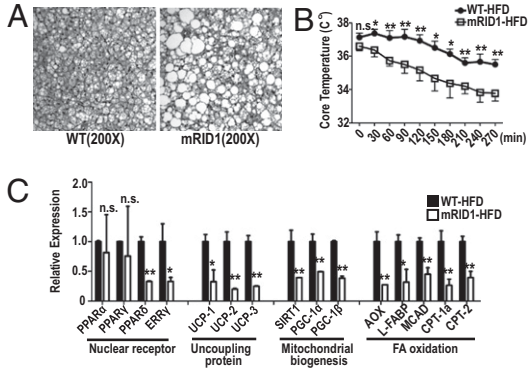

Fig. 4. HFD-challenged SMRT^{mRID1} mice are hypothermic. (*A*) Hematoxylin and eosin staining of BAT from WT and SMRT^{mRID1} mice. (*B*) Rectal temperature was measured at indicated times in WT and SMRT^{mRID1} mice at 4 °C. (*C*) Gene expression of nuclear receptors, thermogenesis and mitochondrial biogenesis, and FA oxidation in BAT from WT and SMRT^{mRID1} mice. All error bars are SD. *$P < 0.05$; **$P < 0.01$; n.s., not significant.

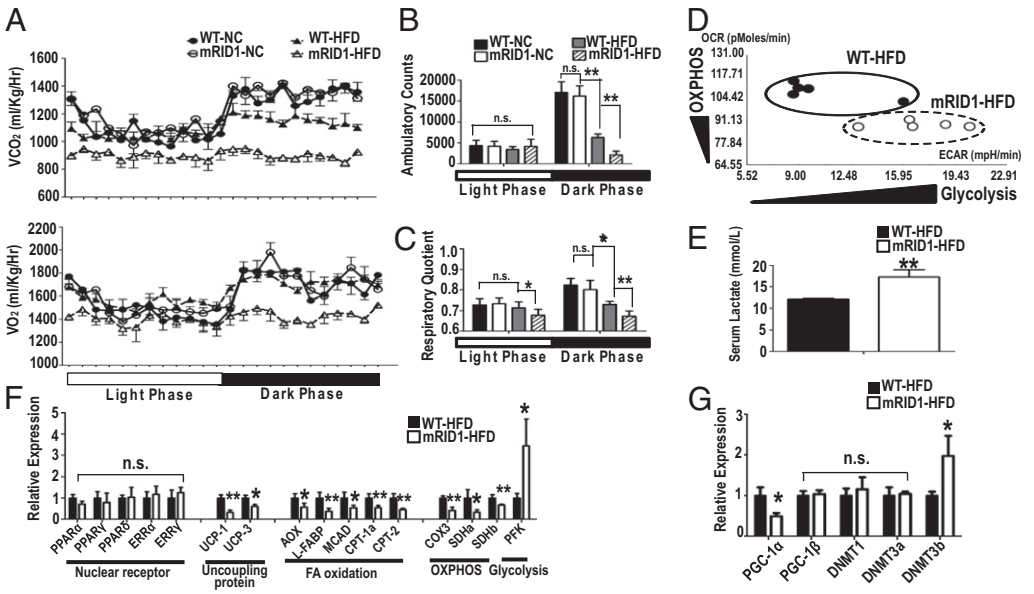

Fig. 5. SMRT^{mRID1} mice are less active, expend less energy, and are more glycolytic than oxidative. (*A*) Carbon dioxide production (*Upper*) and oxygen consumption (*Lower*). (*B*) Cumulative ambulatory counts in WT and SMRT^{mRID1} mice. (*C*) RQ in WT and SMRT^{mRID1} mice. (*D*) Cellular bioenergetics in SVF cells from WT and SMRT^{mRID1} mice. (*E*) Fasting serum lactate level in WT and SMRT^{mRID1} mice. (*F* and *G*) Gene expression of NRs, uncoupling protein, FA oxidation, OXPHOS, glycolysis, PGC1α and -β, and DNMTs in skeletal muscles from WT and SMRT^{mRID1} mice. All error bars are SD. $*P < 0.05$; $**P < 0.01$; n.s., not significant.

target genes attenuates the innate immune response to dietary stressors. Mice harboring a liver-specific disruption of NCoR–NR interactions have recently been described (12). Gene expression analysis described in this study reveals activation of TR (FAS and SCD-1) and LXR (CYP7A1) target genes, implicating overlapping roles for both SMRT and NCoR in maintaining liver metabolic function.

Our data suggest that SMRT-mediated repression of NR signaling is required for the maintenance of metabolic homeostasis during high-fat feeding; loss of repression of a subset of NRs in the SMRT^{mRID1} mice led to aberrant lipid accumulation. Epidemiological studies have identified excessive visceral, but not subcutaneous, fat depots as a risk factor for metabolic dysfunction; however, the biochemical rationale for this difference remains unclear. In the HFD-fed SMRT^{mRID1} mice, the s.c. inguinal fat pads exhibited increased adiposity but decreased expression of inflammatory cytokines, whereas the visceral mesenteric fat pad was hypertrophic and more inflamed (Fig. 1*H*). Gene expression analysis revealed elevated PPARγ expression in all fat pads analyzed. Interestingly, unlike DKI mice, expression of the PPARγ target genes, such as AP2 and CD36, was markedly reduced in visceral fat pads (Fig. S8), suggesting that selective disruption of the RID1 domain could lead to aberrant PPARγ signaling in a fat-depot–specific manner. One could postulate that this is a result of increased occupancy of SMRT on PPARγ sites, which is a consequence of reduced interactions of SMRT with other NRs. The insulin sensitizer, rosiglitazone, is a potent PPARγ agonist that reduces blood glucose level. However, the SMRT^{mRID1} mice were refractory to rosiglitazone treatment unlike the DKI mice (Fig. 3*I*). We speculate that genetic derepression of PPARγ signaling along with enhanced visceral adiposity and chronic inflammation makes this tissue insensitive to Rosiglitazone treatment. Thus, SMRT^{mRID1} mice may identify SMRT as a unique genetic determinant of fat-depot–dependent adipose function.

Defective cellular energy metabolism has been reported as a major contributor to obesity (19), suggesting that mitochondria dysfunction is relevant for the pathophysiology of obesity. This mitochondrial dysfunction is compatible with the defective fatty acid oxidation that is normally observed in obese patients (20). Recently, it was reported that TNF-α, which is overproduced in WAT and muscle tissues in obese patients (21), acts as a regulator of mitochondrial biogenesis (22). Defective TNF-α signaling in WAT, BAT, and muscle partially restored mitochondrial biogenesis (22), suggesting that inflammation plays a critical role in regulating energy metabolism. Given that the expression level of TNF-α was markedly increased in visceral WAT in SMRT^{mRID1} mice (Fig. 1), SMRT-mediated repression of NR signaling appears critical to maintain metabolic homeostasis and is protective against diet-induced inflammation.

In this study, we have characterized a unique mouse model in which disruption of NR–SMRT corepressor interactions through mutations in the RID1 domain caused diet-induced superobesity and reduced energy consumption. The similarities of the diet-induced metabolic dysregulation observed in SMRT^{mRID1} mice with human metabolic disorders suggest that this model may be a valuable tool for investigating abnormal NR-mediated cellular responses in obesity and type 2 diabetes in the context of metabolic syndrome disease. Likely disrupted NR pathways in this model include RARs, TRs, and the PPARs. In particular, future studies focusing on fat-depot–specific mechanisms of SMRT/AMPK may provide important insights into unique mechanisms regulating the physiological controls of energy homeostasis with implications for glucose and lipid metabolism. Finally, the results from this study suggest that NR-mediated repression through SMRT is necessary to balance fat storage versus energy expenditure when presented with high-fat dietary stress.

Materials and Methods

Animal Studies. SMRT^{mRID1} knock-in mice were generated by mutating the ISEVI motif in RID1 encoded by exons 39 and 40 to ASEAA through site-specific mutagenesis. All animal experiments were performed with age-matched male mice from heterozygote crosses that were backcrossed seven times with C57BL/6J to generate a pure genetic background. Mice were maintained in a pathogen-free animal facility under standard 12-h light/12-h dark cycle. For diet-induced obesity, 8-wk-old WT and SMRT^{mRID1} mice were fed with either normal rodent chow (Labdiet 5001; 4.5% fat, 4 kcal/g) or a high-fat diet (Bio-Serv F3282; 35.5% fat, 5.45 kcal/g) for 14 wk. Body

weight was recorded every week. For the cold exposure study, core body temperature was measured with a clinical rectal thermometer (Thermalert model TH-5; Physitemp) every 30 min until mice showed hypothermia. Total cholesterol, TG, insulin, FFAs, leptin, ALT, and adiponectin were determined using enzymatic reactions. For hepatic lipid analysis, the lipid was extracted following the Folch method and resuspended in PBS containing 5% Triton X-100. For GTTs, overnight-fasted mice received 2 g of glucose/kg body weight via i.p. injection. For GTT with rosiglitazone and AICAR, mice received 5 mg/kg of rosiglitazone or 250 mg/kg of AICAR before GTT. Human insulin (Humilin, Eli Lily) was used for ITT. Tail blood was drawn at the indicated time intervals, and blood glucose level was measured with a One Touch Ultra glucometer (LifeScan). For histology, 5-μm sections were stained with hematoxylin and eosin. Statistics were performed by Student's *t* test. Values were presented as means and SDs. All protocols for mouse experiments were approved by the Institutional Animal Care and Use Committee of The Salk Institute.

Body Composition and Adipocyte Size. Body composition was measured with an Echo MRI-100 body composition analyzer (Echo Medical Systems). Total adipose tissue from each depot was excised, and the wet weight was determined. All adipose tissues were fixed in 10% formalin, sectioned, and stained in hematoxylin and eosin. An adipocyte cross-sectional area was determined from photomicrographs of epididymal, mesenteric, and inguinal fat pads using ImageJ.

In Vivo Metabolic Phenotype Analysis. Real-time metabolic analyses were conducted in a Comprehensive Lab Animal Monitoring System (Columbus Instruments). CO_2 production, O_2 consumption, RQ (relative rates of carbohydrate versus fat oxidation), and ambulatory counts were determined for six consecutive days and nights, with at least 24 h for adaptation before data recording.

Gene Expression Analysis. Total RNA was isolated from mouse tissues using TRIzol reagent (Invitrogen) as per the manufacturer's instructions. mRNA levels were quantified by quantitative PCR with SYBR Green (Invitrogen). cDNA was synthesized from 1 μg of DNase-treated total RNA by using SuperScript II reverse transcriptase (Invitrogen). Samples were run in technical triplicates, and relative mRNA levels were calculated by using the standard curve methodology and normalized against 36B4 mRNA levels in the same samples.

Extracellular Flux Bioenergetic Assay. All procedures followed the manufacturer's instructions (Seahorse Bioscience). Briefly, a SVF was isolated from white adipose tissues of WT and $SMRT^{mRID1}$ mice using collagenase type I (Sigma). Cells were seeded in extracellular flux 24-well cell culture microplates (Seahorse Bioscience) at 1.0×10^4 cells/well in 500 μL of growth medium and then incubated at 37 °C/5% CO_2 for 24 h. A Seahorse Bioscience instrument (model XF24) was used to measure the rate of change of dissolved O_2 and pH in the media surrounding the cells. Assays were initiated by removing the growth medium from each well and replacing it with 600 μL of prewarmed assay medium. The microplates were incubated at 37 °C for 30 min to allow media temperature and pH to reach equilibrium before measurement. OCR and ECAR were measured simultaneously for 3–5 min. The values of OCR and ECAR were normalized by the number of cells to reflect the metabolic activities of the cells.

ACKNOWLEDGMENTS. We thank J. Alvarez and S. Kaufman for technical assistance, Chih-Hao Lee for advice and discussion, G. Barish for reagents, and E. Ong and S. Ganley for administrative assistance. R.M.E. is an Investigator of the Howard Hughes Medical Institute at the Salk Institute and March of Dimes Chair in Molecular and Developmental Biology. J.M.S. is supported by an American Diabetes Association fellowship. This work was supported by National Institutes of Health Grants DK062434 and HD027183, the Helmsley Charitable Trust, the Glenn Foundation, the Samuel Waxman Foundation, and the Howard Hughes Medical Institute.

1. Hotamisligil GS (2006) Inflammation and metabolic disorders. *Nature* 444:860–867.
2. Monteiro R, Azevedo I (2010) Chronic inflammation in obesity and the metabolic syndrome. *Mediators Inflamm* 2010:289645–289655.
3. Shulman AI, Mangelsdorf DJ (2005) Retinoid x receptor heterodimers in the metabolic syndrome. *N Engl J Med* 353:604–615.
4. Perissi V, Aggarwal A, Glass CK, Rose DW, Rosenfeld MG (2004) A corepressor/coactivator exchange complex required for transcriptional activation by nuclear receptors and other regulated transcription factors. *Cell* 116:511–526.
5. Jepsen K, et al. (2007) SMRT-mediated repression of an H3K27 demethylase in progression from neural stem cell to neuron. *Nature* 450:415–419.
6. Privalsky ML (2004) The role of corepressors in transcriptional regulation by nuclear hormone receptors. *Annu Rev Physiol* 66:315–360.
7. Perissi V, Jepsen K, Glass CK, Rosenfeld MG (2010) Deconstructing repression: Evolving models of co-repressor action. *Nat Rev Genet* 11:109–123.
8. Nagy L, et al. (1999) Mechanism of corepressor binding and release from nuclear hormone receptors. *Genes Dev* 13:3209–3216.
9. Hu X, Lazar MA (1999) The CoRNR motif controls the recruitment of corepressors by nuclear hormone receptors. *Nature* 402:93–96.
10. Cohen RN, et al. (2001) The specificity of interactions between nuclear hormone receptors and corepressors is mediated by distinct amino acid sequences within the interacting domains. *Mol Endocrinol* 15:1049–1061.
11. Nofsinger RR, et al. (2008) SMRT repression of nuclear receptors controls the adipogenic set point and metabolic homeostasis. *Proc Natl Acad Sci USA* 105:20021–20026.
12. Astapova I, et al. (2008) The nuclear corepressor, NCoR, regulates thyroid hormone action in vivo. *Proc Natl Acad Sci USA* 105:19544–19549.
13. Xu H, et al. (2003) Chronic inflammation in fat plays a crucial role in the development of obesity-related insulin resistance. *J Clin Invest* 112:1821–1830.
14. Kim JJ, Sears DD (2010) TLR4 and insulin resistance. *Gastroenterol Res Pract* 2010:212563–212574.
15. Inflammation PL, Astrom RE, Feigh M, Pedersen BK (2010) Persistent low-grade inflammation and regular exercise. *Front Biosci (Schol Ed)* 2:96–105.
16. Rodgers JT, et al. (2005) Nutrient control of glucose homeostasis through a complex of PGC-1alpha and SIRT1. *Nature* 434:113–118.
17. Pan D, Fujimoto M, Lopes A, Wang YX (2009) Twist-1 is a PPARdelta-inducible, negative-feedback regulator of PGC-1alpha in brown fat metabolism. *Cell* 137:73–86.
18. Barrès R, et al. (2009) Non-CpG methylation of the PGC-1alpha promoter through DNMT3B controls mitochondrial density. *Cell Metab* 10:189–198.
19. Boudina S, et al. (2005) Reduced mitochondrial oxidative capacity and increased mitochondrial uncoupling impair myocardial energetics in obesity. *Circulation* 112:2686–2695.
20. Kim JY, Hickner RC, Cortright RL, Dohm GL, Houmard JA (2000) Lipid oxidation is reduced in obese human skeletal muscle. *Am J Physiol Endocrinol Metab* 279:E1039–E1044.
21. Hotamisligil GS, Arner P, Caro JF, Atkinson RL, Spiegelman BM (1995) Increased adipose tissue expression of tumor necrosis factor-α in human obesity and insulin resistance. *J Clin Invest* 95:2409–2415.
22. Valerio A, et al. (2006) TNF-alpha downregulates eNOS expression and mitochondrial biogenesis in fat and muscle of obese rodents. *J Clin Invest* 116:2791–2798.